Black Box Identification of Earth's Climate System

Philippe de Larminat

Black Box Identification
of Earth's Climate System[*]

Philippe de Larminat[**]

* Submitted to E&E (Energy and Environment journal)
** Independent Scientist. He was Professor at Ecole Centrale, Nantes, France

Abstract

Climate models allow simulating and evaluating the responses of Earth's climate to imbalance factors (known as forcing factors): human, volcanic and solar activities. The purpose of this paper is to assess the respective contributions of these factors only from observations, modern or paleoclimatic, without resorting to any *a priori* quantification of energy flows generated by forcing factors, nor of the coefficients of sensitivity of global temperatures to these energy fluxes.

For this purpose, an energy balance model is calibrated from classical *identification* techniques (in the sense of systems theory). It is a *black box* approach, i.e. based exclusively on observations. Despite the diversity and relative inaccuracy of the models obtained, the simulated contributions of the forcing factors are found to be incompatible with the generally accepted levels. The sensitivity to solar activity appears to be underestimated in a ratio up to 6 or 15; volcanic activity is overestimated at least in a ratio of two. More importantly, the contribution of human activity to recent warming could be negligible compared to that of the internal climate variability. These results are based on objective probabilities, directly derived from observations, which in science prevail over any theoretical speculation. Although they must obviously be received with caution, they cannot be ignored, and we conclude by giving some explanations to the deviations from the prevailing consensus.

** Philippe de Larminat *(Graduate Engineer, 1964, Ph. D., 1972). He was Professor at the Institut National des Sciences Appliquées (Rennes, France) and Ecole Centrale (Nantes). He is the author of 6 books and more than 100 papers in journals and international conferences. Since 2001, he is an independent consultant and author of several patents (e.g. power plants control, satellite guidance). His research interests include mathematical modeling, system identification, signal processing and control theory. Since 2012, he is conducting a pioneer work on identification of the Earth climate system.*

Table of contents

1. Introduction

1.1. Paper's content

This paper continues the effort initiated by de Larminat (2014, 2016) on identification of Earth's climate system. It is organized as follows. After the present introduction, which deals with objective and subjective probabilities, section 2 develop a simplified energy balance model (EBM) which is identifiable from millennial global climate data. Radiative forcing data for human, volcanic and solar activities are detailed in Section 3. The output observations – global surface temperature and ocean heat content – are presented in section 4, and in section 5, the millennial simulations from an *a priori* defined model are compared with the results of PMIP3[1]. Section 6 discusses *black box* identification of the climate system using the usual output error method (OE). Section 7 is devoted to identification based on *historical* measurements (1850-now). Overall, the results overlap with those of CMIP5 (Coupled Model Intercomparison Project Phase 5), which, like those of PMIP3, are based on *a priori* knowledge models: AOGCM (Atmosphere-Ocean General Circulation Model). The two approaches thus validate each other. This agreement is overturned in section 8, dedicated to identification over the millennial period (850-now). The identified models are the only ones that reproduce millenary climatic events: the Warm Medieval Period and the Little Ice Age. The result is a reduced anthropogenic contribution to modern warming and lower values of the metrics that quantify the climate impact of atmospheric CO_2: ESC (Equilibrium Climate Sensitivity) and TCR (Transient Climate Response). Finally, section 9 attempts to draw some robust conclusions, in spite of the dispersion of results from different climatic data sets.

1.2. Modeling approaches

An analytical approach consists in building models exclusively on pre-established laws, *a priori* quantified. It makes it possible to determine the consequences of potential causes on system outputs and to deduce some global systemic parameters through "*experimentation*" from these models. An emblematic example of which is the *climatic sensitivity* of the global surface temperature equilibrium to a possible doubling of the atmospheric CO_2 concentration. The weakness of these approaches obviously is that of weakest link in the quantification of all the causal chains.

Another way is the *black box* identification approach. It relies exclusively on input-output observations to empirically quantify overall relationships between explanatory variables and presumed effects.

All hybridizations are possible, in particular in readjusting the parameters of a complex given model according to the simulation results, for consistency with observations (J.L. Dufresne et al. 2013) [2], or even with the preconceived results (F. Hourdin et al. 2017)[3].

---

[1] Paleoclimate Modelling Intercomparison Project Phase III, under the aegis of IPCC (Intergovernmental Panel on Climate Change)

[2] Section 2.5: "With the same parameters as in the IPSL-CM5A-LR version, the medium-resolution IPSL-CM5A-MR version was producing a mean temperature warmer by only a few tenths of a degree. *It was thus decided to reduce the mean temperature bias in this configuration with a uniform 0.01 increase of the solar absorption coefficient in the ocean*".

[3] "A survey was conducted in August–September 2014, polling 23 different modeling centers that develop coupled atmosphere and ocean models to find out how they tune models. […] 22 of 23 groups reported adjusting model parameters *to achieve desired properties such as radiation balance at the top of the atmosphere*".

In any cases, when dealing with the Earth climate system, results may be subject to large uncertainties, which need to be quantified, preferably in probabilistic terms.

1.3. Objective and Subjective Probabilities

For IPCC[4], *"Objective and subjective probabilities are not always explicitly distinguished"*. This statement is the very title of section 2.6.2 of the Third Assessment Report of IPCC (Group II: Impacts, Adaptation and Vulnerability). Coming from a scientist, a quantified probability is usually interpreted as an objective probability, as for the main conclusion of the fifth assessment report (AR5, 2013): "*It is* extremely likely *[95%] that most of the warming observed during the second half of the 20th century is of human origin*". Likewise, in the Summary for PolicyMakers (SPM) of this fifth report, the IPCC updates the Equilibrium Climate Sensitivity (ECS) in these terms: "It *is defined as the change in global mean surface temperature at equilibrium that is caused by a doubling of the atmospheric CO_2 concentration. Equilibrium climate sensitivity is* likely *[66.6 %] in the range 1.5 °C to 4.5 °C (*high confidence*), **extremely unlikely** [5 %] less than 1 °C (*high confidence*) and* very unlikely *[10 %] greater than 6 °C (*medium confidence*). The lower temperature limit of the assessed likely range is thus less than the 2 °C in the AR4, but the upper limit is the same*". See footnote[5] for the above conventions.

Objective probabilities are inherently not negotiable. In fact, regarding the adoption of the SPM by government delegations in Stockholm, (23-26 Sept. 2013), IISD-Earth Negotiation Bulletin (2013)[6] reports: "*On equilibrium climate sensitivity, several delegations, including Australia, the Netherlands and others, noted that the message that the lower limit of the assessed "likely" range of climate sensitivity is less than the 2°C in the AR4 can be confusing to policy makers and suggested noting it is the same as in previous assessments (i.e. 1.5 °C). The Coordinating Lead Authors explained that comparison to each of the previous IPCC assessments would be difficult, and new language was developed adding that the upper limit of the assessed range is the same as in AR4*" – So what is done (see above).

IPCC itself claims that its own assertions are subjective, being always accompanied by assessments that are themselves subjective (probabilities, degree of agreement, level of confidence[5]). In AR3, group II, 2.6, IPCC insists: "*The popular philosophical view of "objective science" as a series of "falsifications" breaks down when it confronts systems that cannot be fully tested". […] "Bayesian" or "subjective" characterization of probability will be more appropriate*". See also Schneider, S. H., & Moss, R., 1999).

---

[4] 'IPCC' will refer here to the collective author of the Assessment Reports (AR), in particular those of the fifth report of Group 1 (Scientifical Basis). It includes the editors of the various chapters, the Technical Summary (TS) and the Summary for PolicyMakers (SPM), i.e. a total of more than 400 people for the AR5 (2013).

[5] In the Summary for Policymakers, the following terms have been used to indicate the assessed likelihood of an outcome or a result: virtually certain 99–100% probability, very likely 90–100%, likely 66–100%, about as likely as not 33–66%, unlikely 0–33%, very unlikely 0–10%, exceptionally unlikely 0–1%. Additional terms (extremely likely: 95–100%, more likely than not >50–100%, and extremely unlikely 0–5%) may also be used when appropriate. Assessed likelihood is typeset in italics, e.g., *very likely.*

In this Summary for Policymakers, the following summary terms are used to describe the available evidence: limited, medium, or robust; and for the degree of agreement: low, medium, or high. A level of confidence is expressed using five qualifiers: very low, low, medium, high, and very high, and typeset in italics, e.g., *medium confidence*. For a given evidence and agreement statement, different confidence levels can be assigned, but increasing levels of evidence and degrees of agreement are correlated.

[6] http://enb.iisd.org/vol12/enb12581e.html.

For example, the authors refer to a "*runaway greenhouse effect*": the AGW (*Anthropic Global Warming*) could be a completely new event in the history of our planet, and climate behavior would be completely disrupted. Then logic would require that accepted notions such as climate reaction or equilibrium sensitivity be irrelevant, and that it would be futile to try to learn anything from paleoclimate science. Rather than going that far, it can be assumed that, even if human action is unprecedented, prior climate laws subsist, and that millenary paleoclimatic data are of sufficient duration for the ergodicity hypothesis to apply. The result is a *frequentist* vision that does not have to be depreciated as *a popular philosophical view*. The applicability of the time invariance and ergodicity assumptions to internal climate variability remains questionable, as do the observation times for asymptotic approximations, but the *black box* identification approach applied to the climate system is by nature objective: the calibration of models and uncertainties comes from observations and observations alone. Data and methods can be challenged, but not the scientific principle whereby observations take precedence over subjectivity.

2. Development of an energy balance model

2.1. Basic principles

The ingredients in the following model are trivial, they are only arranged in order to lead to a simplified Energy Balance Model (EBM), adjustable through a minimum number of parameters, so that it can be identified from input-output data. It is a two-compartment model: atmosphere and oceans. Their respective states are the mean surface temperature T_S and the ocean heat content Q_O.
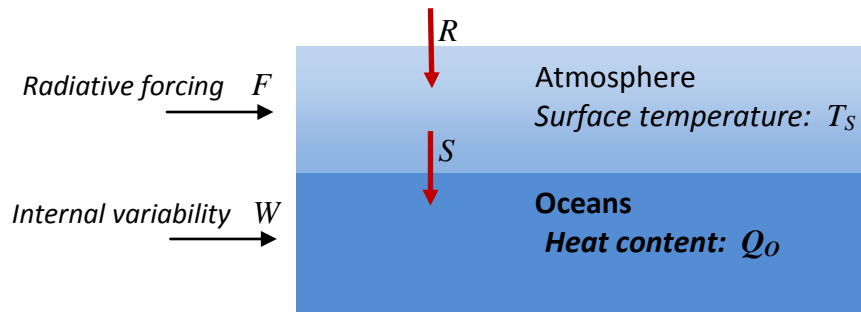
Figure 1. *A basic Energy Balance pattern*

A universally accepted expression (Budyko, 1969; Sellers 1969, Hansen 2005, Geoffroy et al. 2013) for the energy balance R at the top of the atmosphere (TOA) is as follows:

$$R = F - \lambda(T_S - T_{PI}) \tag{1}$$

The radiative balance R (in Wm^{-2}) is zero at the climatic equilibrium. F is the total radiative forcing induced by external factors of climate imbalance (human, volcanic and solar actions). Its components are evaluated against a pre-industrial reference (typically the 850-1850 baseline). T_{PI} is the resulting pre-industrial equilibrium temperature and λ is a climatic feedback coefficient ($Wm^{-2} \ ^\circ C^{-1}$). In a Simplified Climate Model (SCM) context, λ is assumed to be an independent parameter, although according to Hansen (2005), it could depend on the type of forcing F.

The heat flow S through the surface depends on the two climatic states T_S and Q_O. It is clear that S is increasing with T_S. For Q_O, it's the opposite. Hence a linearized formulation:

$$S = \mu(T_S - T_{PI}) - \nu(Q_O - Q_{PI}) + W \tag{2}$$

Through equation (2), the coefficients μ ($Wm^{-2}/{}^\circ C$) and ν ($year^{-1}$) determine the heat transfer flow S. This expression neglects the transients induced by the inertia of the superficial oceanic layers. In addition, a disturbance term W appears, which locates in equation (2) the involvement of internal climate variability resulting from the chaos of atmospheric and oceanic circulations, their interactions, and the temperature redistributions within the oceans.

Lastly, the usual assumption that the thermal inertias of the atmosphere and continental surfaces are negligible is made explicit. They do not store heat, and the R and S energy flows are therefore permanently equalized. Hence the evolution of ocean heat:

$$dQ_O / dt = S = R \tag{3}$$

2.2. State equations and transfer function

Equations (1), (2) and (3) define an implicit dynamic model. The independent signals (causes) are F and W. An explicit model follows from the formal solution of the system (1, 2, 3), where dQ_O / dt and T_S are the unknowns. The solution is written as:

$$d(Q_O - Q_{PI}) / dt = \frac{\lambda}{\lambda + \mu}\left(-\nu(Q_O - Q_{PI}) + \mu\left(\frac{F}{\lambda}\right) - W\right) \tag{4}$$

$$(T_S - T_{PI}) = \frac{1}{\lambda + \mu}\left(\nu(Q_O - Q_{PI}) + \lambda\left(\frac{F}{\lambda}\right) + W\right) \tag{5}$$

Equations (4) and (5) now define an explicit dynamic system described by *state space equations*, of the form $dx/dt = Ax + Bu$, $y = Cx + Du$, state variable $x = Q_O - Q_{PI}$, input variables $u = [F; W]$, output variable T_S. Conversion into a *transfer function*, where the Laplace variable s symbolizes the operator d/dt (Schwarz, R. J., & Friedland, B., 1965, de Larminat, P., 2009), gives:

$$(T_S - T_{PI}) = \frac{1 + \rho s T_{\text{clim}}}{1 + s T_{\text{clim}}}\left(\frac{F}{\lambda}\right) + \frac{\rho s T_{\text{clim}}}{1 + s T_{\text{clim}}}\left(\frac{W}{\mu}\right) \tag{6}$$

where : $T_{\text{clim}} = \dfrac{\lambda + \mu}{\lambda \nu}$ and $\rho = \dfrac{\mu}{\lambda + \mu}$ \hfill (7)

The equilibrium sensitivity of the climate system to a unit variation in radiative forcing (RFS: *Raditive Forcing Sensitivity*) is $1/\lambda$ and noted as S_{RF}:

$$S_{RF} = 1/\lambda \quad (\text{in } {}^\circ C/Wm^{-2}). \tag{8}$$

This sensitivity is obviously different from ECS (*Equilibrium Climatic Sensitivity*), whose name and acronym in use don't specify that they refer to the sensitivity to a doubling of CO_2.

2.3. Comments

– Despite its simplicity and fertility, equation (2) is not commonly used by climate scientists. Its interest is to directly lead to a simplified model that can be interpreted as the ultimate reduction of a multilayer model, where all the thermal inertias would tend towards 0, with the exception of that of the oceans. However, it differs fundamentally from ordinary first-order models in that the atmosphere and oceans are not amalgamated into a single element: T_S and Q_O remain distinct.

– The model transients are characterized by the transfer function $G(s) = (1 + \rho s T_{\text{clim}}) / (1 + s T_{\text{clim}})$. It is of unit static gain, and the numerator $(1 + \rho s T_{\text{clim}})$ involves an instantaneous transmission of radiative forcings to the T_S output, thus approximating the short-term response found in all the models of higher complexity (see Figure 2).

– In the state form as well in transfer function, the model is parameterized by three coefficients λ, μ, ν (or through the equivalent triplet λ, T_{clim}, ρ), plus the pre-industrial values T_{PI} and Q_{PI}.

– Equations (5) and (6) imply that the rapid variations of W instantly affect the temperature, and also R through equation (1). Nevertheless, the static gain of the second term of (6) is zero: if W drifts during millennia, this drift will not appear on T_S.
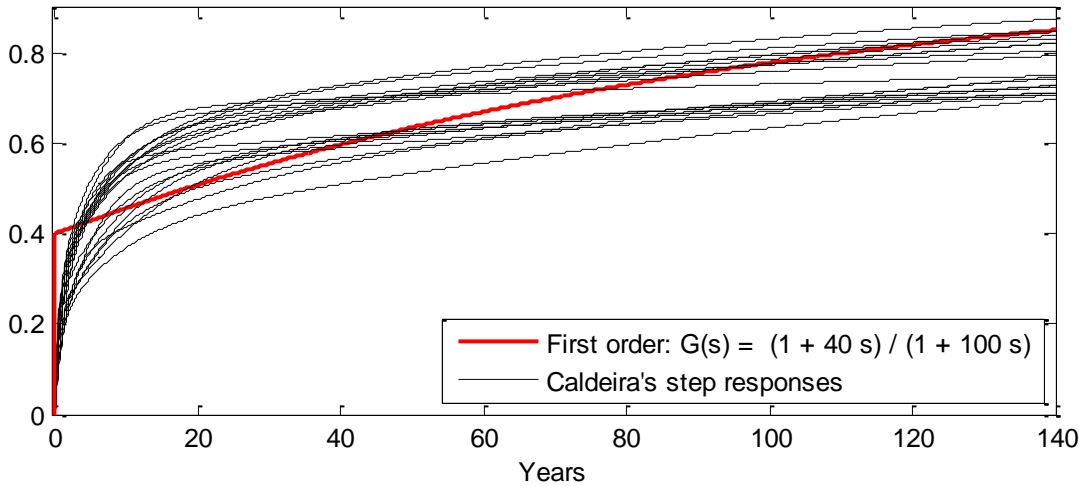
Figure 2. *First order approximation of 20 AOGCM step responses (Caldeira,* 2013*)*

3. Radiative forcings

3.1. Quantification of radiative forcings

The transfer function $G(s)$ defines the dynamic part of the model. Repartition and quantification of radiative forcings are the static part. The total radiative forcing F, renamed F_{tot}, is broken down into:

$$F_{tot} = F = F_{anth} + F_{volc} + F_{sol} \tag{9}$$

The F_{xxx} are respectively the anthropogenic, volcanic and solar contributions to total forcing. These forcings are evaluated from historical and/or paleoclimatic measurements. With the exception of TSI (Total Solar Irradiance), the measurements are not directly expressed in Wm^{-2}. Determining radiative forcings may be based on the fundamental laws of physics (thermodynamics, fluid mechanic, etc.). More often, physical laws are empirical (optical depth of aerosols, vapor oversaturation in clouds, etc.).

8

These modes may be combined. For example, Myrhe (1998) stated that a variation of atmospheric CO_2 concentration of C_1 to C_2 produces, to within a few percent, a radiative forcing of $3.7 \log_2(C_2/C_1)$ Wm^{-2}. Sometimes, they sin by omission, as for the indirect mechanisms of action of solar activity. In addition, the measures themselves vary according to the sources.

Within the framework of the CMIP5 and PMIP3 projects, the IPCC provides participants with millennial series of radiative forcing. These radiative forcings f_{xxx}, are referred to as *A Priori* Forcings (APF), to differentiate them from the real forcings F_{xxx} (eq. 9).

In a context of determining the respective contributions of forcing factors to climate variations, the static part of the model (distribution of radiative forcings) plays a major role with respect to the dynamic part, the diversity of AOGCM or EBM having only a minor impact on the overall result. Taking the validity of these APFs for granted would amount to ratify in advance the resulting distribution of climate variations.

Thus, the real radiative forcings will be assumed to be equal to $F_{xxx} = a_{xxx} \times f_{xxx}$, where the scaling factors a_{xxx} should be close to 1, but are to be determined as the other coefficients of the model.

3.2. A priori forcings (APF)

The *a priori* forcings used here are shown in Figure 3 and are almost identical to those in Figure 8.18 of AR5 (2013). The zero reference of forcings is 1850.
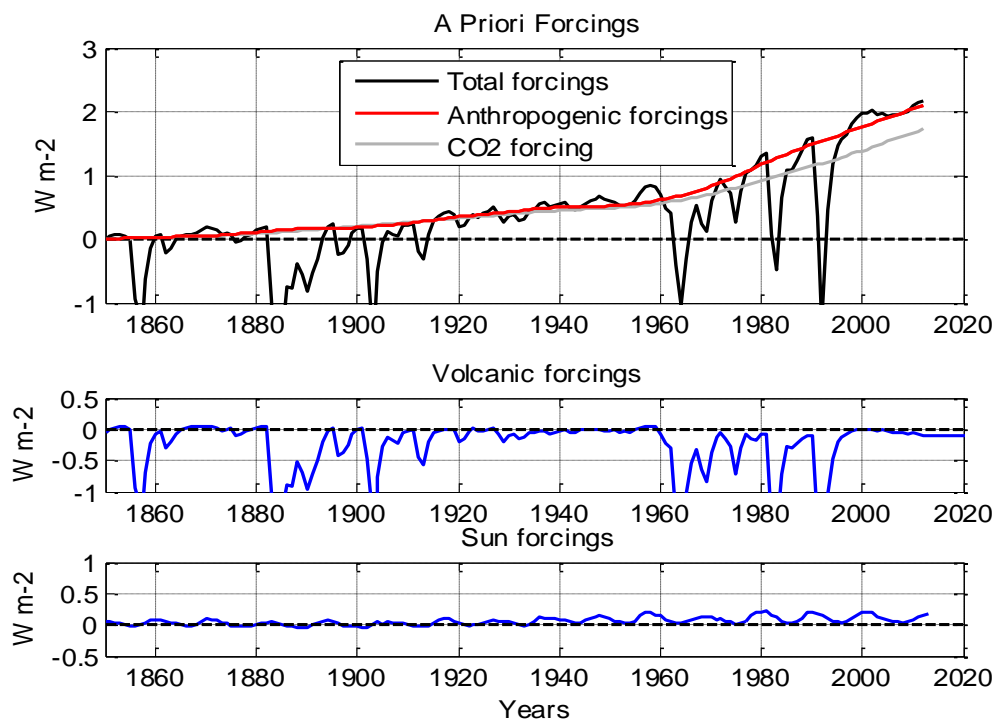
Figure 3. *Given a priori forcings*

Total anthropogenic forcing results from greenhouse gases, industrial aerosols, land use changes, etc. Forcings depends on the data sources. For example, the total anthropogenic forcing of Miller (2014) put online by NASA for CMIP5 is 30% higher than that in Figure 8.18 of the AR5. Hence the need to estimate the multiplicative coefficient a_{anth}.

Through compensations between GHGs, aerosols and land use changes, the anthropogenic total differs little from the CO_2 *a priori* forcing (fig 3-a). It also differs from it in the natural variations of CO_2 prior to the industrial era, and which must be taken into account when estimating CO_2-based

metrics (ESC and TCR). Finally, we adopt as *a priori* anthropogenic forcing factor the expression of Myrhe: $f_{anth} = 3.7 \log_2(C/C_{PI})$ (Wm^{-2}).

Volcanic forcing connects the PMIP3 data (Crowley, 2013), since 850 and CMIP5 data (Sato, 1993), from 1850. They were initially expressed in AOD (*Aerosol Optical Depth* at 550 *nm*), and Miller multiplies them by a factor of 26 for conversion to Wm^{-2}. Other authors prefer lower factors (20 for example).

Solar forcing: Miller's (2014) data can be superimposed on Schmidt's (2010) and SOLARISHEPPA's data[7]. Figure 4 shows two possible solar forcing f_{sol}: *weak and strong variability*. The bold lines show the smoothed series. Miller retained the high variability forcing, which remains low in absolute terms (see fig. 3). Both these APFs lead all the CMIP5 participants to insignificant solar contributions to the simulated global temperatures.
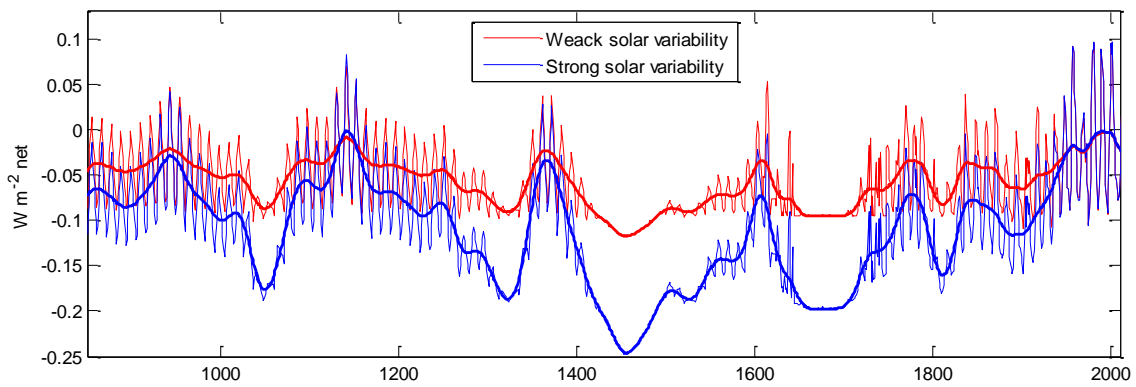

Figure 4. *Solar net forcings*

The Low-Frequency variations (LF, bold lines) are obtained by smoothing and are practically proportional to each other (ratio 2.2), while the High-Frequency complements (HF), consisting mainly of Schwabe cycles (about 11 years), are identical from one series to another. Figure 5.1-b of AR5 shows other reconstructions (Lean 2000, Shapiro, 2011), where the ratio of LF/HF components may reach about ten.

In all the signals relating to solar activity (sunspots, spectral irradiance, heliocentric magnetic field, geomagnetic field, solar wind, radio background noise, etc.), the LF and HF components are respectively similar, but in different proportions. All these manifestations can potentially impact the climate through indirect mechanisms distinct from the direct energy flow. As a result, total solar forcing cannot be derived by proportionality from a single indicator.

Our solution consists in introducing *two distinct solar forcing indicators f_{Lsol}* and *f_{Hsol}*, defined as the LF and HF components of one signal, *a priori* representative of the global solar activity (we adopt here the strong TSI variability of Figure 4).

Note1. The composite reconstructions in Figure 4 are based on satellite observations (since 1978), combined with sunspot observations and cosmogenic proxies. The differences in Figure 4 result from the variety of solar models used by solar scientists.

Note2. There are no observations or proxies with sufficient resolution to build up a millennium HF forcing. The HF components in Figure 4, prior to 1610, are "*synthetic*" reconstructions. The HF amplitudes are plausible, being based on that of the LF components. On the other hand, the phase has

no reality, being associated with fictitious solar cycles of periods strictly equal to 11 years. The indicator f_{Hsol} can therefore be significant only from 1610 onwards.

Finally, the total radiative forcing is written:

$$F_{tot} = a_{anth} f_{anth} + a_{volc} f_{volc} + a_{Lsol} f_{Lsol} + a_{Hsol} f_{Hsol} \qquad (10)$$

This expression completes the model. The coefficients a_{anth}, a_{volc}, a_{Lsol} and a_{Hsol} are to be determined, as well as the dynamic parameters T_{clim}, ρ, and the sensitivity to radiative forcing $S_{RF} = 1/\lambda$.

As shown in equations (4, 5, 6), the input-output data f_{xxx} and T_s allow to estimate only the a_{xxx}/λ ratios. To individualize a_{xxx} and λ an additional measure is required: It will be the ocean heat content Q_O.

4. Global climate observations

4.1. Global mean surface temperature

There are many historical measurements and paleoclimatic reconstructions of global average surface temperature. A very complete source is Pangaea (V. Masson-Delmotte et al., 2013). It comprises a total of 23 distinct series, grouped by hemispheres (see AR5, fig. 5.7). We have retained the 14 millenary paleoclimatic series available without distinction[8]. Figure 5 shows the average of these 14 reconstructions, connected to the Hadcrut4 series for the historical period. The baseline is the pre-industrial average (851-1850).
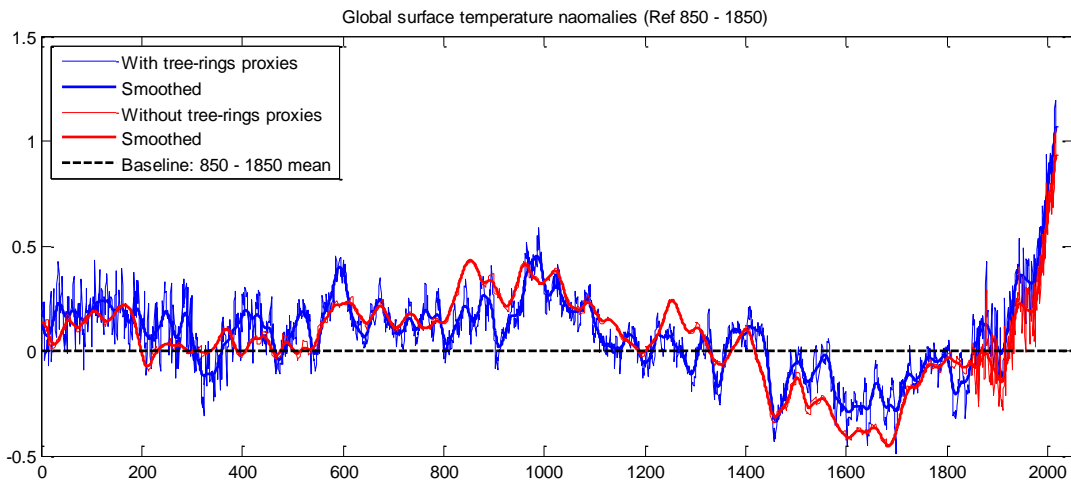
Figure 5. *Temperature reconstructions: all proxies and without tree-rings*

Most paleoclimatic reconstructions involve as proxies the annual growth rings of trees, famous since the reconstruction of M. Mann et al (1999), the *Hockey Stick Graph*. Very popular in the early 2000s, this curve is now excluded from the references cited by AR5. In addition, long-lived species (britlescone pines) are often found at the edge of their natural habitat, for example in Siberia (Yamal

---

[7] Solar Powering America by Recognizing Communities (SPARC)

peninsula) or at high altitudes (California). They are therefore not necessarily representative of the global terrestrial climate. In addition, tree-rings are sensitive to conditions other than temperature (especially hydric). In a context of recurrent problems of modern divergence with thermometric measurements (D'Arrigo, 2008, Loehle, C. 2009), the selection of samples from Yamal (Siberia) has been controversial[9]. Tree-rings are assumed to benefit from a good annual resolution. Yet they detect virtually no reaction to the largest volcanic eruption of our era (Samalas, 1257). Given their low sensitivity to long-term climatic variations, they must be exploited in conjunction with other proxies (^{18}O isotopes in sediments, etc.) Under these conditions, tree-rings do not appear to be a proxy of decisive interest.

Only two of the above temperature reconstructions do not use tree-rings, those of Ljungqvist (2009) and Loehle (2007). Their average, connected to the historical HadCRUT4 observations, is shown in Figure 5 and will be used for comparison with the first one. It is noted that tree-rings tend to reduce temperature excursions during the warm medieval period (850-1200) and the little ice age (1400-1850).

4.2. Ocean heat content

The second measure regarding the global climate effects is the Oceans Heat Content (OHC). An interesting feature of our model is that it appears as a state variable in the model (éq. 4, 5). The earliest estimates begin in the 1950s. Accuracy gradually improved until the 1990s, mainly with the development of the Argo system in the 2000s. Figure 6 shows the data collected by Cheng (2019). The total ocean heat content Q_O is expressed in ZJ (10^{21} *Joules*). For consistency with climatic units, it is converted[10] into *Watt* x *year / square meter* (Figure 6)
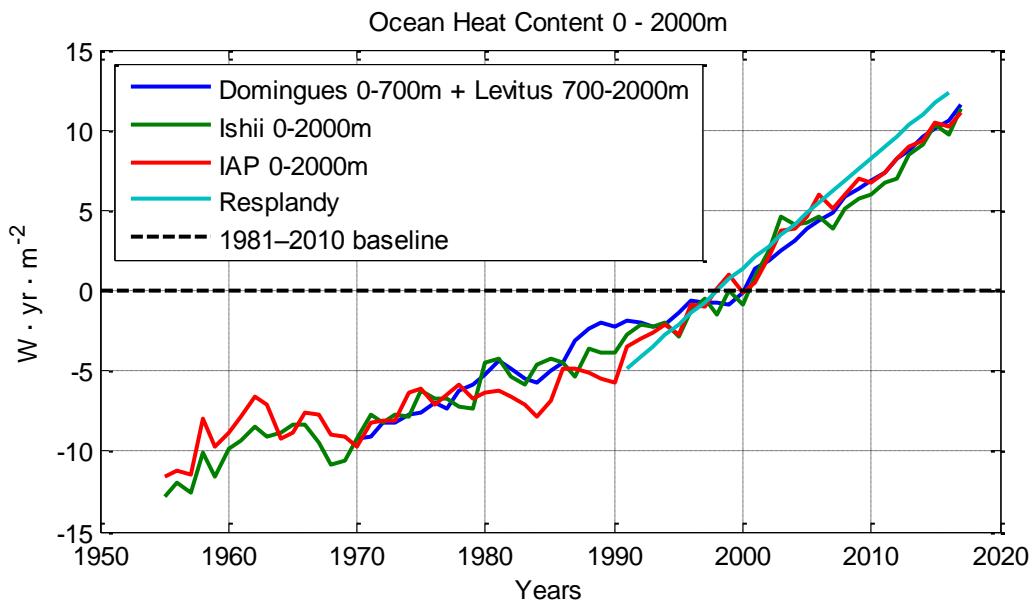
Figure 6. *Ocean Heat Content -OHC*

---

[8] *Pangaea* d*esignation*: CL12loc, Da06treecps, Fr07treecps, He07tls, Ju07cvm, LM08ave, LO12glac, Lj10cps, Ma08cpsl, Ma08eivf, Ma08eivl, Ma08min7eivf, Ma09regm, Mo05wave, Sh13pcar.
[9] https://www.theguardian.com/environment/2010/feb/09/yamal-climate-tree-ring-data-withheld
[10] Without reproducing the mistake of G. Smith, who had reduced the entire earth surface to that of the oceans http://www.realclimate.org/index.php/archives/2012/05/ohc-modelobs-comparison-errata/

5. *A priori* simulations

5.1. A priori *forcings and models*

For these first simulations, we adopt the APFs as inputs (i.e. $a_{xxx} = 1$). A good agreement with those of PMIP3 is obtained by arbitrarily setting $\lambda = 0.8$, $T_{c\lim} = 100$ *years* and $\rho = 0.2$.

Forcing data are uncertain or missing during the first centuries of our era. In addition, the system has no reason to be in equilibrium in Year 1 when starting simulations. Like does PMIP3, we assume that the initial transients are extinguished before the beginning of the observation period (year 850).

5.2. *Paleoclimate simulation*

Figure 7 is based on [FigBoxTS5-1-b](#) in the AR5 Technical Summary, in which the visualization of reconstructions are limited to the grey levels representative of some confidence index. For more clarity, we add (grey line) the associated centre of gravity, close to the average of the reconstructions shown in Figure 5 (all proxies). Furthermore, we follow PMIP3 which adopts the Little Ice Age (1450-1850) as the baseline for simulations and reconstructions.
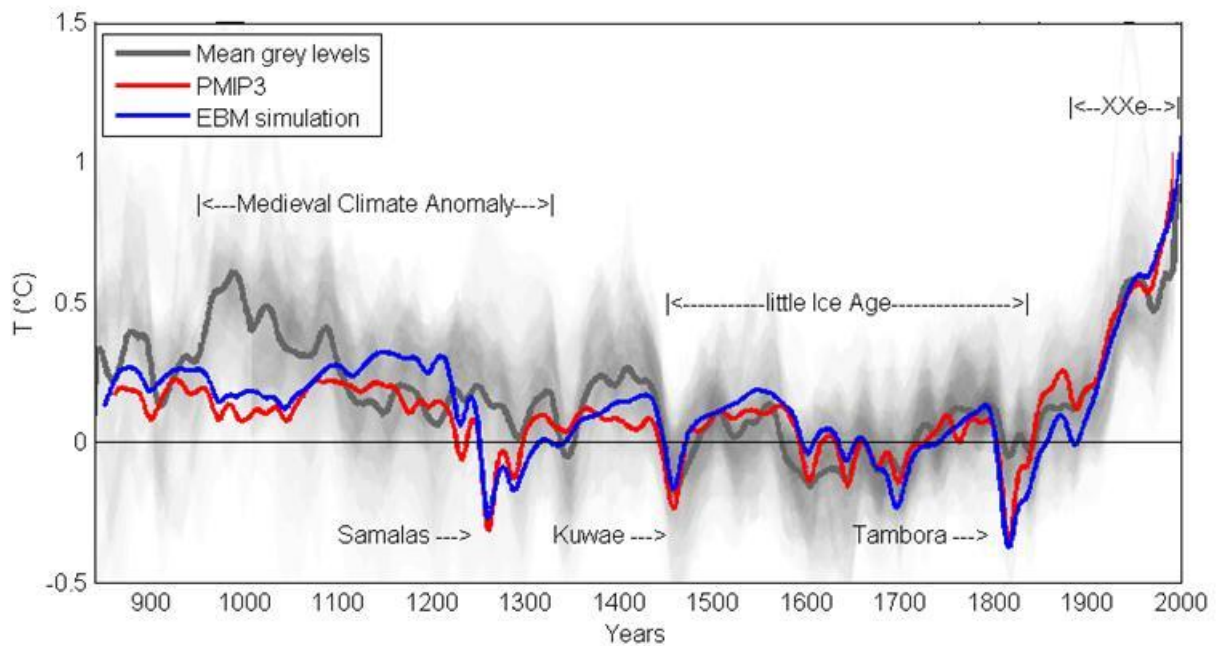
Figure 7. *Comparison PMIP3 – EBM*

Comments

− Similarity is surprising, between the average of a set of AOGCM simulations (red) carried out by multiple centers, and that of a single, roughly calibrated model (blue). This similarity is primarily due to identity of the radiative forcing at the input of the models.

− Unavoidably, the maximum proximity between the three lines arises during the common baseline (the Little Ice Age: 1450-1850).

− At the end of the 20th century, the simulated temperatures are significantly higher than the observed temperatures. The choice of the baseline tends to make this defect less visible. It could be due to an overestimation of the anthropogenic radiative forcing, but the temperatures shown in Figure 7 are not measured temperatures, but proxies-based reconstructions, some of which presenting problems of divergence with modern observations (D'Arrigo, et al. 2008).

− A disappointing reproduction of the medieval warm period is observed, suggesting an underestimation of the low-frequency component of solar radiative forcing. This defect is less flagrant in the AR5 Figures, where the solid grey curve is omitted.

− The model reactions to volcanic forcing are questioning. In 1257 (eruption of the Samalas), temperature reconstructions (grey) show no significant repercussion on the real climate, while simulations exhibit a considerable impact, indicating a strong overestimation of the volcanic APF. This overestimation is less obvious at the eruptions of Kuwae (1453) and Tambora (1809) which are accompanied by temperature drops. These can also be explained by the minimum solar activity of Spörer and Dalton, contemporaneous of these eruptions.

Clearly, all these combined over- and under-estimates in the APFs go in the same direction: they minimize both the contribution of the modern solar maximum to present warming, and the failure of GCMs to reproduce the climate over millennial period.

5.3. Oceans Heat Content simulations

The OHC simulations consist in integrating the radiative balance through the TOA (eq. 1). S is determined by the T_S observations and the *a priori* forcing F over the observation period. T_{PI} is the *a priori* pre-industrial temperature (850-1850 average of T_S).

$$Q_O(t) = Q_O(t_1) + \int_{t_0}^{t} (F - \lambda(T_S - T_{PI})) dt \,, \quad t \in = [t_1, \ t_2] \tag{11}$$

Let us first consider (Figure 8, in blue), the result obtained with $\lambda = 0.8$, previously used for the T_S simulations. It is growing faster than the average of the observations (in grey). The difference can be interpreted as a "missing heat" (Tollefson, J., 2014), in relation to the sum of the TOA radiation balance, if *a priori* assumed to be accurate. This missing heat could be hidden in the abyss, or on the surface of continents, or as latent heat exchanged with the cryosphere (Katsman, C. V., & van Oldenborgh, G. J. 2011). This could explain at most a few percent of the deficit. Other explanations can be sought, for example an underestimation of the reaction coefficient λ. So, the red plot shows the better simulation performed with $\lambda = 1.5$.
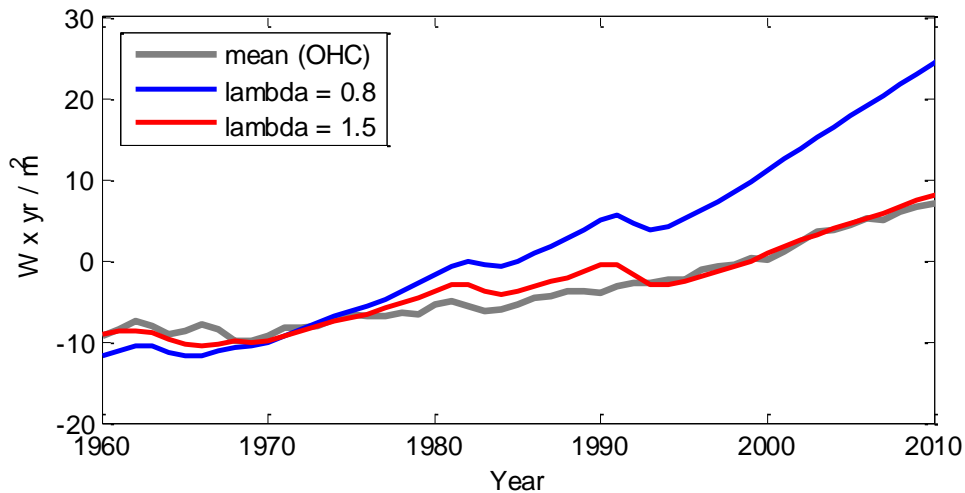

Figure 8. *Ocean Heat Content: observation and simulations*

Simulations show a visible impact of eruptions from the volcanoes Agung (1964), el Chinchon (1981) and Pinatubo (1991). It is less noticeable on the average of the observations. Modern

observations of OHC therefore confirm the overestimation of volcanic APFs, already observed during the paleoclimatic period.

In the following sections, the a_{xxx} scale factors as well the λ coefficient will be estimated using dynamic systems identification techniques, where the results will be dictated exclusively by the T_S and Q_O climate observations, without any *a priori* quantification of a_{xxx}, either physical or coming from a consensus that precisely requires validation.

6. Climate system identification

6.1. Identification

Identification covers the theory of estimation applied to causal dynamic systems. It has emerged as an autonomous discipline since the First IFAC Symposium on System Identification (Praha, 1967). It is most often applied for automatic control purpose to manufactured systems on which it is possible to experiment by acting on the input variables, more rarely to natural systems where the input signals cannot be manipulated.

The main contributors to the theory and practice of identification are K. J. Åström (1971) and L. Ljung (1999). Also cited: Soderstrom and Stoïca, (1988); Young, (1981); Walter and Pronzato (1997); Landau (2001); de Larminat (2009). The variety of methods enables to achieve statistical optimality (ARMAX, B&J, PEM methods, etc.) or to simplify implementation (OLS).

6.2. Output Error Method

The most intelligible and robust method is the *least squares of output error* (OE), which is directly related to the archetype of estimation methods: the least squares of Carl Friedrich Gauss (1777 - 1855).

In our case, it consists in simulating the model fed by the *a priori* forcings and in minimizing with respect to the parameters the mean squares of the differences between the simulated outputs and the observed or reconstructed T_S and Q_O outputs. Given the simplicity of the model and the small number of parameters (including the a_{xxx} scale factors), numerical simulations and minimizations are easily achieved.

Concerning T_S, the a_{xxx} scale factors appear only through quantities $S_{xxx} = a_{xxx} / \lambda$, where S_{xxx} are the equilibrium climatic sensitivities with respect to the four APF f_{xxx}. Sensitivities S_{xxx} are therefore directly identified, which would all be equal to $S_{RF} = 1 / \lambda$ in the ideal case of scale factors equal to 1. Dynamic parameters T_{clim} and ρ, as well as the pre-industrial equilibrium temperature T_{PI} are also identified.

Quantities T_{clim} and ρ formally depend on λ (eq. 7), but the dependence is too weak for deducing λ or S_{RF}. This will be done through the Q_O measurement.

6.3. Variance of estimations

It is known that the OE method is statistically optimal (asymptotically unbiased and minimal variance) when noise and disturbances are reduced to a white noise additive on the output. This is not the case here, particularly because of the contribution of internal climate variability.

This optimality deficit (the greater the minimization interval, the lower this deficit), is nevertheless compatible with a calculation of the variance of the estimator (Appendix), involving the autocorrelation function of the output error.

In addition to their inherent interest (confidence intervals), the estimated variances allow Monte-Carlo simulations, based on random realizations of the estimated parameters. The ranges of natural and anthropogenic contributions can then be visualized and compared with those of the IPCC.

6.4. Estimating the feedback climate coefficient

The short observation period of the ocean heat content Q_O does not allow to expect a significant improvement to the parameters already estimated through T_S. However, it provides the additional information required to estimate the climate reaction coefficient λ. Equations (1) and (3) are rewritten under the form:

$$dQ_O / dt = F - \lambda(T_S - T_{PI}) \tag{12}$$

We denote as ΔQ_O the increase in Q_O over a finite time interval Δt, for example 1990-2010. We note $\bar{F}$ $\bar{T}_S$ and $\bar{f}_{xxx}$ the mean values of F, T_S and f_{xxx} over the time interval Δt. Hence the equation:

$$\Delta Q_O / \Delta t = \bar{F} - \lambda(\bar{T}_S - T_{PI})$$

where $\bar{F} = \lambda(S_{anth}\bar{f}_{anth} + S_{volc}\bar{f}_{volc} + S_{Lsol}\bar{f}_{Lsol} + S_{Hsol}\bar{f}_{Hsol})$

Hence the expression of λ:

$$\lambda = \frac{\Delta Q_O / \Delta t}{S_{anth}\bar{f}_{anth} + S_{volc}\bar{f}_{volc} + S_{Lsol}\bar{f}_{Lsol} + S_{Hsol}\bar{f}_{Hsol} - (\bar{T}_S - T_{PI})} \tag{13}$$

The means $\bar{f}_{xxx}$ are those of the APFs. ΔQ_O and $\bar{T}_S$ are given by the observations. As a function of the estimated variables S_{xxx} and T_{PI}, which are involved in the denominator, the variable λ potentially has a heavy tail distribution, for which the concepts of mean value or variance are not relevant.

On the other hand, the notions of median and quantiles are meaningful and can be determined by the Monte-Carlo method. In practice, the random realizations of S_{xxx} and T_{PI} are obtained from the calculated estimates and variances under the Gaussian assumption. When expression (13) leads to a negative λ value, and therefore to an unstable model, it is excluded. At the same time, $S_{RF} = 1 / \lambda$, $a_{xxx} = S_{xxx} / \lambda$ are determined.

Estimates are then defined as the medians of the various variables, with *probable* (66%) or *very likely* (90%) confidence intervals.

The *a priori* contribution of CO_2 to anthropogenic forcing is $f_{2\times CO2} = 3.7\log_2(C / C_{PI})$. To obtain $S_{2\times CO2}$, *the sensitivity to equilibrium at the doubling of* CO_2, we apply the estimated scale factor a_{anth}: $S_{2\times CO2} = a_{anth}3.7 / \lambda$. Note that this relation holds only for each Monte-Carlo trial, not for the medians.

7. Identification over the historical period

7.1. Parametric estimation

The length of the historical period (1850-2010) is of the same order as the climatic time constant T_{clim}. It is therefore illusory to try to estimate it. The values $T_{\text{clim}} = 100 \; yrs$ and $\rho = 0.2$, compatible with the subsequent results of the millennium identification (section 8) are taken again here. Minimization of the output error on T_S allows identifying the APFs climate sensitivities S_{xxx}, as well as the variance of the estimates. Then, the observation of the OHC allows determining the factors λ and a_{xxx}, as well as the Equilibrium Climate Sensitivity.

	Median	*Likely* (66.6 %)	
λ :	1.03	[0.90 1.49]	$Wm^{-2}/°C$
ECS :	3.26	[2.03 4.58]	$°C$
a_{anth} :	0.99	[0.76 1.17]	–
a_{volc} :	**0.34**	**[0.20 0.53]**	–
a_{Lsol} :	1.28	[-2.14 5.99]	–
a_{Hsol} :	0.42	[-0.58 1.38]	–

Table 1. *Historical identification*

The *likely* confidence intervals of the a_{xxx} scale factors all include unity, with the exception of the volcanic scale factor, which confirms the overestimation of the corresponding APF.

7.2. Simulations

Figure 9-a shows the CMIP5 simulations. It reproduces Figure 10-21 of AR5. The uncertainty ranges reflect the dispersion of simulations performed by all PMIP3 participating centers, not the uncertainties on the given APFs.

Below (9 b), we have the simulations resulting from the parameters identified by minimizing the output error over the historical period. In thin lines, the Monte-Carlo simulations carried out on the basis of objective probabilities of the estimated scale factors. Therefore, they have no reason to reproduce the ranges of CMIP5, where the dispersion reflects the individual decisions arbitrarily taken by each participant (see above footnotes 2 and 3).

It must be noted that the identified volcanic impact is significantly lower than that reported by the CMIP5.
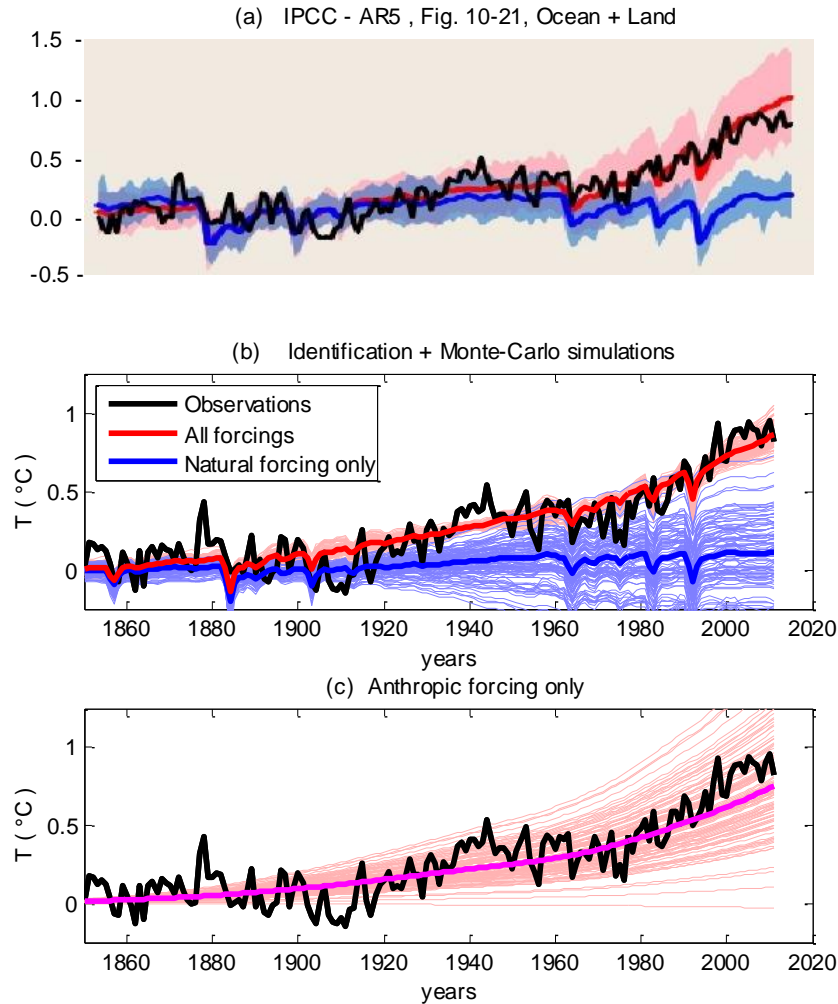
Figure 9. *Historical period identification*

For the moment, figure 9-c goes in line with the SPM's assertion that most of the warming observed during the second half of the 20th century is human-induced.

7.3. Millennial hindcast

The simulations carried out for identification over the historical period are started at Year 1, in a zero initial state, and are feed by the millenary inputs f_{xxx}. It is assumed that the transient errors are extinguished in 850, *a fortiori* in 1850, the starting date of the optimization period. Figure 9 is limited to the historical period, although Figure 10-a shows the entire simulation over the millennium period 850-2010. It is identical to 9-b over the historical period. The plots were only filtered for comparison with Figure 6.

The model identified over the historical period shows no tendency to reproduce either the warm medieval period or the small ice age. Figure 6 could be seen as more satisfactory. This was due to the artifices of overestimating volcanic activity and centering on the Little Ice Age. Conversely, the simulation based on the identified model does not show any anomaly related to millennial volcanic eruptions, even when they lie outside the identification period.
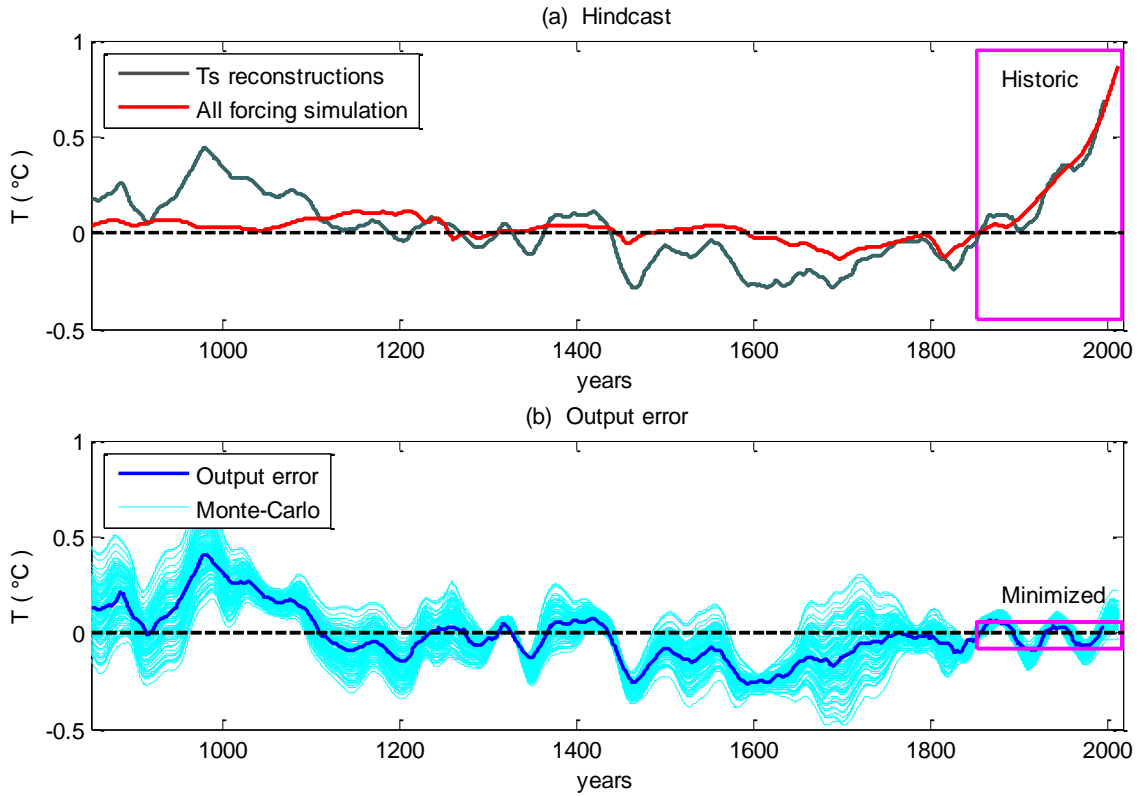
Figure 10. *Hindcast: Simulations from identification over the historical period*

Figure 10-b shows the output error. The disproportion between the amplitudes of the minimized deviations and the hindcast deviations is explained by: 1) errors in the measurement and reconstructions of T_S, which were more important in the paleoclimatic era, 2) internal variability, 3) an extremely simplified model structure. The historical period is obviously affected from the last point, which may be predominant.

Note. It appears some periodicity over the historical period. In view of the whole millennium deviation, it is difficult to decide whether this cyclicality on two periods only is fortuitous or not.

7.4. Comments

Whatever the explanations used, any error minimized over too short a period underestimates the statistical characteristics of noise and disturbances. The uncertainties on the identified parameters, calculated on the basis of the output error, limited to modern times, are therefore probably underestimated.

It is therefore not possible to draw any serious conclusions from the identification over the historical period, either on the value of the identified parameters or on their confidence intervals. This criticism also concerns *detection and attribution* (Hegerl, 2010) applied to the human origin of global warming, when it is limited to the same historical period, or even to the shorter period of satellite observations (de Larminat, 2016).

8. Millennium identifications

The millennium identification (850-2010) remains based on the same APF, but we consider the two types of paleoclimatic reconstructions of T_S temperature successively: *all proxies* and *without tree-*

rings. The long duration of the observations now makes it possible to estimate the dynamic parameters T_{clim} and ρ.

8.1. Dynamical parametres

The following results are obtained (medians and *likely* ranges):

– *All proxies* identification: $T_{\text{clim}} = 85$ [69, 176] *yrs*, $\rho = 0.10$ [0.01, 0.19].

– *Without tree-rings* identification: $T_{\text{clim}} = 120$ [4, 255] *yrs*, $\rho = 0.12$ [0.03, 0.27].

Figure 11 shows the Monte-Carlo step responses of $G(s) = (1 + s\,\rho\,T_{\text{clim}}) / (1 + s\,T_{\text{clim}})$
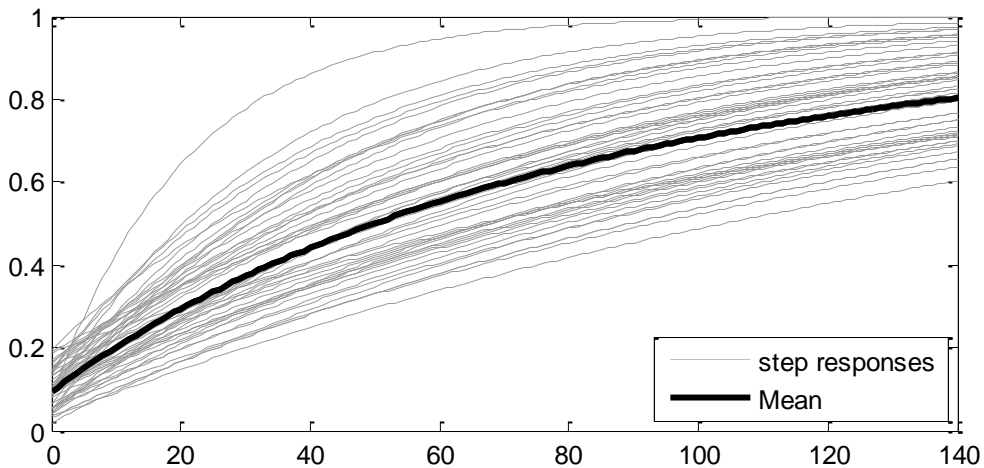

Figure 11. *Identified G(s) (all proxies)*

The identified responses do not match well with these of CMIP5 (Figure 2), which are the result of *a priori* modeled AOGCMs. Oceanic circulation, especially thermohaline plays a major role in modeling atmosphere to ocean exchange (see El Niño) and long-term transients. The deep ocean circulation has been observed over a short period by the Argo system and is still poorly known. Hindsight will be lacking for a long time, before knowledge models are validated. It is therefore not surprising that the transients of the identified models differ significantly from the *a priori* models.

8.2. Millenary identification and simulations

The simulation results (Figs. 12 and 13) should be compared with Figures 8 and 9. From Figure 12, it is seen that taking into account millenary observations leads to attribute a significant part of contemporary warming to natural forcings, and in particular to low-frequency solar activity. There is a better simulation of the medieval warm period and the little ice age (12-c), but there is still a significant output error, indicating high internal variability, even though it does not appear most pronounced in the historical period.
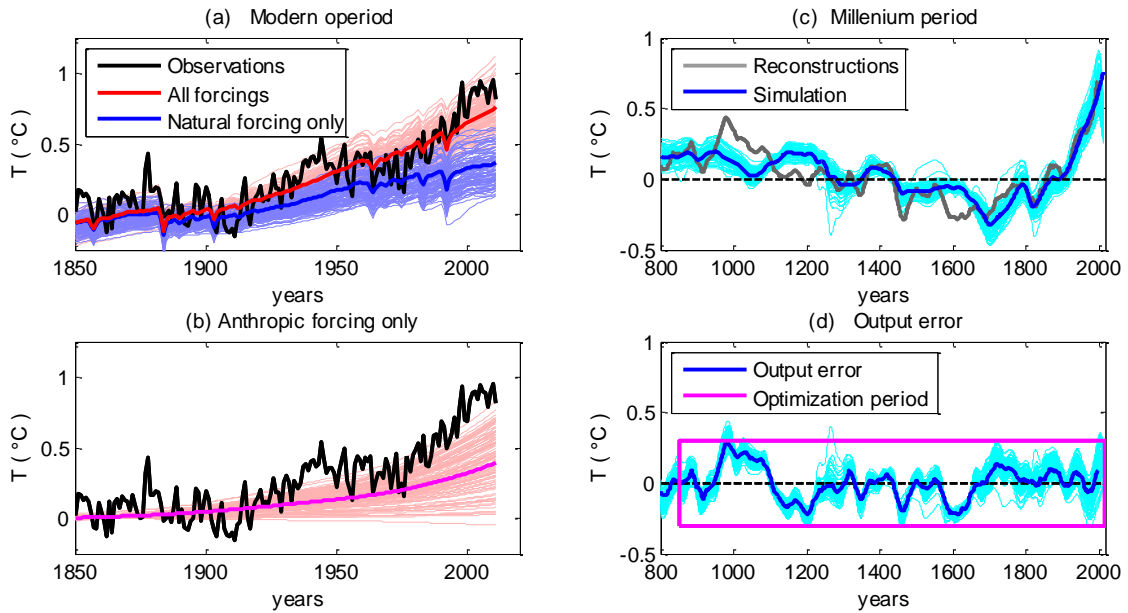
Figure 12. *Simulations, all proxies temperatures.*

Figure 13 (without tree-rings) strongly accentuates the above effects. The reproduction of the millenary temperature is improved, while the modern warming appears to be mainly due to natural forcings. Even the sign of anthropogenic contribution turns out to be questionable.
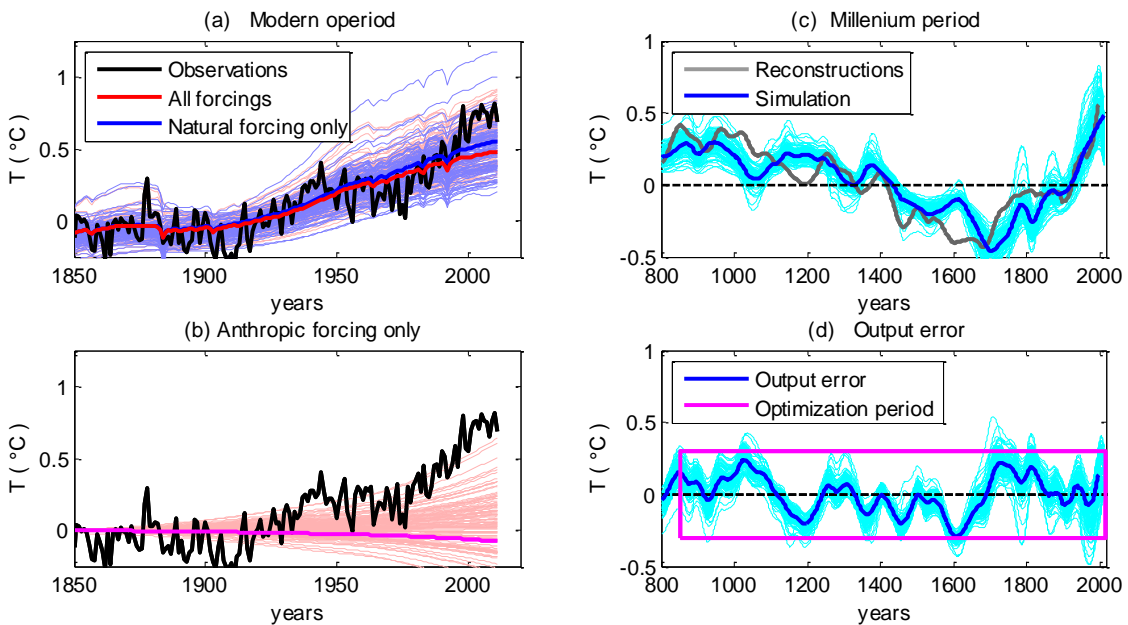
Figure 13. Simulations, without tree-rings proxies

8.3. *Estimated parameters*

Table 2 compares the historical identification with the last paleoclimatic identifications.

|	Historic		All proxies		Without tree-rings	
	Median	66.6 %	Median	66.6 %	Median	66.6 %
λ	1.03	[0.90 1.49]	1.19	[0.67 3.68]	1.47	[0.74 4.22]
a_{anth}	0.99	[0.76 1.17]	0.68	[0.55 1.08]	**0.10**	[-0.75 0.36]
a_{volc}	**0.34**	[0.20 0.53]	0.53	[0.27 1.27]	**0.26**	[0.08 0.84]
a_{Lsol}	1.28	[-2.14 5.99]	**6.07**	[3.16 16.5]	**14.9**	[7.38 42.22]
a_{Hsol}	0.42	[-0.58 1.38]	0.58	[−1.6 2.54]	−0.68	[−3.05 0.27]

Table 2. *Climate feedback and scaling factors*

There are several disagreements with the IPCC's assertions.

– A reduced anthropogenic contribution, possibly negative in the case of identification without tree-rings.

– A lower volcanic impact, even when identifying over the historical period.

– The scale factors identified from millennial observations indicate a radiative forcing by solar activity 6 to 15 times higher than the IPCC *a priori* forcing.

This last point is probably the most dramatic contribution of this study.

8.4. Equilibrium Climate Sensitivity and Transient Climate Response

Climate sensitivities to CO_2 doubling are the most evocative metrics of human action on climate change. In fact, equilibrium sensitivity (ECS) is not really significant, given that the response times involved are multi-secular. Estimates are therefore necessarily very uncertain.

For the Transient Climate Response (TCR) the doubling of atmospheric CO_2 would occur with an increase of 1% per year, i.e. in 70 years ($1.01^{70} \sim 2$). Then TCR is the temperature reached at the end of these 70 years, without waiting for the final equilibrium. TCR is therefore necessarily lower than ECS. It is better suited for human scale assessment and its estimation is potentially more reliable. TCR is obtained from the identified parameters, simulating the response to the above scenario. Medians and ranges are deduced through Monte-Carlo trials.

Figure 13 compares the identified climate sensitivities (lines 1, 2, 3) with the ranges indicated in IPCC reports AR4 and AR5 (when available). From one report to another, the ranges correspond to different confidence intervals; a median or most likely value is not always indicated.
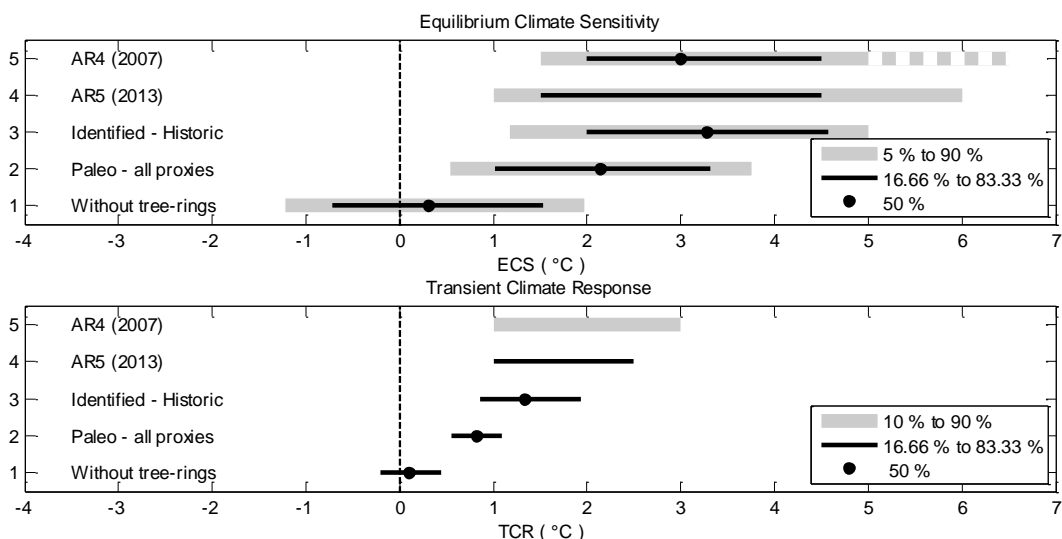
Figure 13. *Climate sensitivity to doubling CO$_2$*

There is no obvious contradiction between the ESC identified over the historical period and the IPCC assessments (lines 3, 4, 5). They are all in the order of 3 °C. On the other hand, the millenary identification from *all proxies* temperatures shows clearly lower low limits. In particular, the *very unlikely* lower limit of AR5 decreases from 1 °C to 0.5 °C. With the identification *without tree-rings*, disagreement is total: the *likely* range is disjoined from that of the IPCC and even the sign of the climate sensitivity becomes uncertain.

For the transient TCR climatic response, the same incompatibilities are found, reinforced by the differences in the dynamics of the transfer function $G(s)$ (Figures 2 and 10). Even if limited to the identification from *all proxies*, a TCR of about 1°C in 70 years, in the pessimistic hypothesis of a doubling of CO$_2$, is likely to substantially reduce the concerns related to the AGW.

9. Discussion

9.1. Caveat

The accuracy of identified models is limited by the conditions of the climatic experience: short observation period, high levels of noises and disturbances.

Confidence ranges are based on assumptions and approximations whose degree of validity is difficult to assess. First, that the deviations between models and observations are dominated by internal variability, assumed to be time invariant while the accuracy of measurement errors varies with age. Second, due to the spectrum of this internal variability, it is difficult to ensure that its correlation function is correctly assessed over a millennium, and that the central limit theorem actually applies. The linearity assumption and the simplified structure of the model may also be questioned. However, our entire approach leads to simple algorithms with are infinitely easier to handle and reproduce than AOGCM simulations.

9.2. Ergodicity

The most critical hypothesis is that of ergodicity: data of various origins are mutually biased, and by nature a bias does not respect ergodicity which conditions the convergence of averages over time towards overall averages. Then, the best way is to present the results coming from different data sets and leave it to each to decide based to decide whether climatic data or reconstructions are reliable, questionable… or worse. It is only at this step that subjectivity finally appears: For example, the AGW would be completely confirmed if we decide to place total confidence in the M. Mann's *hockey stick graph*. Here, our analysis is limited in two different reconstructions of global temperature: from *all proxies* or *without tree rings*. Other analyses would also be necessary: since CMIP5 and PMIP3, new data have emerged and older data have been corrected, with the effect of erasing the "climate pause" observed at the beginning of the 21st century (Karl et al., 2015). In de Larminat (2014, 2016), we also studied the sensitivity to reconstructions of solar activity: indeed, the Sunspot Number count, initiated by Wolf in 1849 and uninterrupted since then, is now suspended in favor of a new count through *Group Numbers* (Clette et al., 2015, Svalgaard et al., 2016), which opportunely reduces the amplitude of the "great solar maximum" of the 20th century.

9.3. Solar impact

Whatever the data set selected, the identification allows an objective arbitration between the causes of global warming. In all cases, simulations show a strong solar contribution in the long term (MWP or

LIA) and in the medium term (at the minima of Spörer and Dalton). The consistency of solar observations with global temperatures over the last millennial strongly suggests a much higher Low-Frequency to High-Frequency ratio than that of the TSI based APFs. There are two explanations. The first is that of the low-frequency forcing is actually higher than that of APFs (see Shapiro, 2011). The second is the existence of other impact mechanisms of solar activity (Soon & al. 2015), for example through the heliocentric magnetic field (Svensmark, 1997, 2017), or the geocentric magnetic field (Courtillot & al. 2007, Le Mouël & al., 2019, Zherebtsov, G.A., 2019), or the solar wind (Landscheidt, T., 2000). The IPCC does not incorporate such mechanisms into AOGCMs due to the lack of *a priori* quantified knowledge. But even though effects are not yet fully understood or evaluated, it does not mean they do not exist. Identification modeling makes their detection possible through the estimate of the a_{Lsol} scale factor. This depends on the selected climate data, but it is always much higher than unity, questioning the low order of magnitude of the solar APFs by IPCC, as well their negligible contribution to the global temperature. On the contrary, our simulated solar impacts may be predominant, in contradiction with the SPM's statement that "it is *extremely likely* (95%) that most of the warming observed in the second half of the 20th century was due to human activity". This announced probability is subjective: it is not based on global climate observations, but on a consensus coming from physical a priori knowledge, mostly arbitrary settled.

9.4. Internal variability

Millennial simulations, from both identified models and IPCC's reveal a high level of *internal variability*, which contributes to explain the modern warming, to the detriment of human action. In fact, at a millennium scale, the internal variability induced by ocean chaos could dominate over external forcings at levels much higher than those observed at the decadal time scale. Where only a few decades of atmospheric observations were sufficient to validate meteorological models, centuries of ocean observations could be needed to reach a real understanding of ocean chaos and its aleas. It is unlikely that this can be achieved in the short term through theoretical models and Navier-Stockes equation simulations. In the meantime, one may wonder about the capacity of climate science, in the current state of art, to make credible secular projections.

10. Conclusion

Millenary climate observations and reconstructions confirm the preponderance of solar activity on large climatic variations, in association with the internal variability of the climate. Conversely, volcanism does not seem to have contributed significantly to the major millenary climatic events: medieval warm period, little ice age and contemporary warm period. For this last one, nothing confirms that human activity is a predominant cause. These conclusions are based on identification of climate parameters and objective confidence domains.

References

AR5 (2013). See IPCC (2013).
Åström, K. J., and Eykhoff, P. (1971). System identification – a survey. *Automatica*, *7*(2), 123-162.
Bard, E., & Delaygue, G. (2008). Comment on "Are there connections between the Earth's magnetic field and climate?" by V. Courtillot, Y. Gallet, J.-L. Le Mouël, F. Fluteau, A. Genevey EPSL 253, 328, 2007. *Earth and Planetary Science Letters*, *265*(1-2), 302-307.
Caldeira, K., & Myhrvold, N. P. (2013). Projections of the pace of warming following an abrupt increase in atmospheric carbon dioxide concentration. Environmental Research Letters, 8(3), 034039.

Cheng, L., J. Abraham, Z. Hausfather, K. E. Trenberth, 2019: How fast are the oceans warming? *Science*, 363, 128-129. doi: 10.1126/science.aav7619.

Clette, F., Svalgaard, L., Vaquero, J. M., & Cliver, E. W. (2015). Revisiting the sunspot number. In *The Solar Activity Cycle* (pp. 35-103). Springer New York.

Courtillot, V., Gallet, Y., Le Mouël, J. L., Fluteau, F., & Genevey, A. (2007). Are there connections between the Earth's magnetic field and climate?. *Earth and Planetary Science Letters*, *253*(3-4), 328-339. https://www.sciencedirect.com/science/article/pii/S0012821X06007667

Crowley, T. J., Zielinski, G., Vinther, B., Udisti, R., Kreutz, K., Cole-Dai, J., & Castellano, E. (2008). Volcanism and the little ice age. *PAGES news*, *16*(2), 22-23.

Crowley, T. J. and M. B. Unterman, (2013), Technical details concerning development of a 1200-yr proxy index for global volcanism. *Earth System Science Data*, Vol. 5.

D'Arrigo, R., Wilson, R., Liepert, B., & Cherubini, P. (2008). On the 'divergence problem'in northern forests: a review of the tree-ring evidence and possible causes. *Global and planetary change*, *60*(3-4), 289-305

de Larminat, P. (2009). *Automatique appliquée* (chapitre 13), Paris, Lavoisier.

de Larminat, P. (2014). *Climate Change, Identification and Projections*. Wiley & Son

de Larminat, P. (2016). Earth climate identification vs. anthropic global warming attribution. *Annual Reviews in Control*, *42*, 114-125.

Delaygue, G., and E. Bard (2011) . "An Antarctic view of Beryllium-10 and solar activity for the past millennium." *Climate Dynamics* 36.11-12: 2201-2218.

Dufresne, J. L., Foujols, M. A., Denvil, S., Caubel, A., Marti, O., Aumont, O., ... & Bony, S. (2013). Climate change projections using the IPSL-CM5 Earth System Model: from CMIP3 to CMIP5. *Climate Dynamics*, *40*(9-10), 2123-2165.

Geoffroy, O., Saint-Martin, D., Olivié, D. J., Voldoire, A., Bellon, G., & Tytéca, S. (2013). Transient climate response in a two-layer energy-balance model. Part I: Analytical solution and parameter calibration using CMIP5 AOGCM experiments. *Journal of Climate*, *26*(6), 1841-1857.

Hansen, J. E., Sato, M. K. I., Ruedy, R., Nazarenko, L., Lacis, A., Schmidt, G. A., ... & Bell, N. (2005). Efficacy of climate forcings. *Journal of Geophysical Research: Atmospheres*, *110*(D18).

Hansen J, Lacis A, Rind D, Russell G, Stone P, Fung I, Ruedy R and Lerner J (1984) Climate sensitivity: analysis of feedback mechanisms Climate Processes and Climate Sensitivity (*Geophysical Monograph Series* vol 29) ed J. E. Hansen and T. Takahashi (Washington, DC: American Geophysical Union) pp 130–63

Hegerl, G. C. et al. (2010). Good practice guidance paper on detection and attribution related to anthropogenic climate change. *In Meeting Report of the Intergovernmental Panel on Climate Change Expert Meeting on Detection and Attribution of Anthropogenic Climate Change* (p. 8). IPCC Working Group I Technical Support Unit, University of Bern, Bern, Switzerland.

Hourdin, F., Mauritsen, T., Gettelman, A., Golaz, J. C., Balaji, V., Duan, Q., ... & Rauser, F. (2017). The art and science of climate model tuning, B. Am. Meteorol. Soc., 98, 589–602.

Hoyt, D. V. and Schatten, K. H., (1998): Group sunspot numbers: A new solar activity reconstruction. *Solar physics*, 181(2), 491-491

IISD-Earth Negotiation Bulletin (2013), *D. Understanding the climate system and its recent changes* Volume 12, Number 581

Imbers, J., Lopez, A., Huntingford, C., & Allen, M. R. (2013). Testing the robustness of the anthropogenic climate change detection statements using different empirical models. *Journal of Geophysical Research: Atmospheres*, *118*(8), 3192-3199.

IPCC, 2013: Climate Change (2013): The Physical Science Basis. Contribution of Working Group I to the Fifth Assessment Report of the Intergovernmental Panel on Climate Change [Stocker, T.F., D. Qin, G.-K. Plattner, M. Tignor, S.K. Allen, J. Boschung, A. Nauels, Y. Xia, V. Bex and P.M. Midgley (eds.)]. *Cambridge University Press,* Cambridge, United Kingdom and New York, NY, USA, 1535 pp.

Karl, T. R., Arguez, A., Huang, B., Lawrimore, J. H., McMahon, J. R., Menne, M. J., ... & Zhang, H. M. (2015). Possible artifacts of data biases in the recent global surface warming hiatus. *Science*, *348*(6242), 1469-1472.

Katsman, C. V., & van Oldenborgh, G. J. (2011). Tracing the upper ocean's "missing heat". *Geophysical research letters*, *38*(14).

Landscheidt, T. (2000). Solar wind near Earth: Indicator of variations in global temperature. In *The Solar Cycle and Terrestrial Climate, Solar and Space weather* (Vol. 463, p. 497).

Le Mouël, J. L., Lopes, F., Courtillot, V., & Gibert, D. (2019). On forcings of length of day changes: From 9-day to 18.6-year oscillations. *Physics of the Earth and Planetary Interiors*, *292*, 1-11.

Ljung, L. (1998). *System identification* (pp. 163-173). Birkhäuser Boston.

Ljungqvist, F.C. (2009). N. Hemisphere Extra-Tropics 2,000yr Decadal Temperature Reconstruction. IGBP PAGES/*World Data Center for Paleoclimatology Data Contribution Series #* 2010-089. NOAA/NCDC Paleoclimatology Program, Boulder CO, USA.

Loehle, C., (2007), "A 2000-years global temperature reconstruction based on non-treering proxies", *Energy & Environment*, Vol. 18, No. 7+8

Loehle, C. (2009). A mathematical analysis of the divergence problem in dendroclimatology. *Climatic Change*, *94*(3-4), 233-245.

Mann, Michael E., Raymond S. Bradley, and Malcolm K. Hughes. (1999) "Northern hemisphere temperatures during the past millennium : Inferences, uncertainties, and limitations." *Geophysical Research Letters* 26: 759-762.

Masson-Delmotte, Valerie; Schulz, Michael; Abe-Ouchi, Ayako; Beer, Jürg; Ganopolski, Andrey; González Rouco, Jesus Fidel; Jansen, Eystein; Lambeck, Kurt; Luterbacher, Jürg; Naish, Timothy R; Osborn, T; Otto-Bliesner, Bette L; Quinn, Terrence Michael; Ramesh, Rengaswamy; Rojas, Maisa; Shao, XueMei; Timmermann, Axel (2013): *Information from Paleoclimate Archives*. *PANGAEA*, https://doi.org/10.1594/PANGAEA.828636

Masson-Delmotte, V., M. Schulz, A. Abe-Ouchi, J. Beer, A. Ganopolski, J.F. González Rouco, E. Jansen, K. Lambeck, J. Luterbacher, T. Naish, T. Osborn, B. Otto-Bliesner, T. Quinn, R. Ramesh, M. Rojas, X. Shao and A. Timmermann, (2013): *Information from Paleoclimate Archives*. In: AR5 (2013).

Miller, R. L., et al. (2014), CMIP5 historical simulations (1850–2012) with GISS ModelE2, J. Adv. Model. Earth Syst., 6, 441–478, doi:10.1002/2013MS000266.

Myhre, Gunnar, *et al*. "New estimates of radiative forcing due to well mixed greenhouse gases." *Geophysical research letters* 25.14 (1998) : 2715-2718.

Sato, M., Hansen, J. E., McCormick, M. P., & Pollack, J. B. (1993). Stratospheric aerosol optical depths, 1850–1990. *Journal of Geophysical Research: Atmospheres*, 98(D12), 22987-22994.

Scafetta, N., & Willson, R. C. (2014). ACRIM total solar irradiance satellite composite validation versus TSI proxy models. *Astrophysics and Space Science*, *350*(2), 421-442.

Schmidt, G. A., Jungclaus, J. H., Ammann, C. M., Bard, E., Braconnot, P., Crowley, T. J., ... & Otto-Bliesner, B. L. (2012). Climate forcing reconstructions for use in PMIP simulations of the Last Millennium (v1. 1). Geoscientific Model Development, 5, 185-191.

Schneider, S. H., & Moss, R. (1999). Uncertainties in the IPCC TAR: Recommendations to lead authors for more consistent assessment and reporting. *Unpublished document*.

Schwarz, R. J., & Friedland, B. (1965). *Linear systems*. McGraw-Hill.

Söderström, T., and Stoica, P. (1988). *System identification*. Prentice-Hall, Inc.

Soon, W., Connolly, R., & Connolly, M. (2015). Re-evaluating the role of solar variability on Northern Hemisphere temperature trends since the 19th century. *Earth-Science Reviews*, *150*, 409-452.

Svalgaard, L. and Schatten, K. H. (2016). Reconstruction of the sunspot group number: the backbone method. *Solar Physics*, *291*(9-10), 2653-2684.

Svensmark, H., Enghoff, M. B., Shaviv, N. J., & Svensmark, J. (2017). Increased ionization supports growth of aerosols into cloud condensation nuclei. *Nature communications*, *8*(1), 2199.

Svensmark, H., & Friis-Christensen, E. (1997). Variation of cosmic ray flux and global cloud coverage—a missing link in solar-climate relationships. *Journal of atmospheric and solar-terrestrial physics*, *59*(11), 1225-1232.

Taylor, K. E., Stouffer, R. J., & Meehl, G. A. (2012). An overview of CMIP5 and the experiment design. Bulletin of the American Meteorological Society, 93(4), 485-498.

Tollefson, J. (2014). Climate change: The case of the missing heat. *Nature News*, *505*(7483), 276.

Usoskin, I.G., K. Alanko-Huotari, G.A. Kovaltsov, and K. Mursula, , (2005) Heliospheric modulation of cosmic rays: Monthly reconstruction for 1951-2004, J. Geophys. Res., 110, A12108 (doi:10.1029/2005JA011250)

Usoskin, I. G., Monika Korte, and G. A. Kovaltsov (2008). "Role of centennial geomagnetic changes in local atmospheric ionization." *Geophysical Research Letters* 35.5

Walter, E., and Pronzato, L. (1997). Identification of parametric models. *Communications and Control Engineering*, *8*.

Young, P. (1981). Parameter estimation for continuous-time models—a survey. *Automatica*, *17*.

Zherebtsov, G.A., V.A. Kovalenko, S.I. Molodykh, K.E. Kirichenko (2019) Solar variability manifestations in weather and climate characteristics. *Journal of Atmospheric and Solar-Terrestrial Physics* 182:217–222

Appendix. Estimating the parametric uncertainty variance

Being a process, let's explicit the dependence of the observed output y with respect to a vector θ_0 of parameters by writing:

$$y = f(\theta_0) + v$$

where:

$- y = [y_1 \cdots y_t \cdots y_N]^T$ is the vector of observed outputs, from time $t = 1$ to N

$- f(\theta_0) = [f_1(\theta_0) \cdots f_t(\theta_0) \cdots f_N(\theta_0)]^T$ is the vector of the outputs, which would result from the simulation of the exact model.

$- v = [v_1 \cdots v_t \cdots v_N]^T$ is the deviation, coming from the noises and disturbances on the output, including those from input errors. This sequence is assumed to be identically distributed, ergodic and centered, but not necessarily independent: $E(v_i v_{j \neq i}) \neq 0$.

By definition, he OE estimate $\hat{\theta}$ of θ_0 is that which minimizes the criterion:

$$J(\theta) = \|y - f(\theta)\|^2$$

which can be approximated as:

$$J(\theta) = \|v + f(\theta_O) - f(\theta)\|^2 \sim \|v + F_\theta(\theta_0 - \theta)\|^2$$

where F_θ is the Jacobian matrix of partial derivatives of f at any θ in the vicinity of θ_0. The last term above is minimum for:

$$(\hat{\theta} - \theta_0) = F_\theta^+ v$$

where $F_{\theta_0}^+$ is the pseudo-inverse of F_θ : $F_\theta^+ = (F_\theta^T F_\theta)^{-1} F_\theta^T$.

Hence the approximate expression of the covariance matrix of $\hat{\theta}$:

$$V_{\theta\theta} \sim F_{\theta_0}^+ V_{vv} F_{\theta_0}^+$$

In order to perform this expression, the Jacobian matrix F_θ is computed through finite differences, carrying out n simulations from the OE estimate $\hat{\theta}$, successively varying each component: $\hat{\theta}_i = \hat{\theta}_i + \delta\theta_i$. Under the ergodicity hypothesis, the covariance matrix V_{vv} can be calculated using the autocorrelation function of the residuals $\hat{v} = y - f(\hat{\theta})$:

$$V_{vv}(i, j) \sim \frac{1}{N} \sum_{t=1}^N \hat{v}_t \hat{v}_{t+i-j}$$

Once the covariance matrix $V_{\theta\theta}$ is determined, one can perform all classical analyses: confidence intervals, parametric tests, etc.